
Article:
Castillo Alvarez, Cristina, Penkman, Kirsty orcid.org/0000-0002-6226-9799, Kröger, Roland orcid.org/0000-0002-5070-0297 et al. (4 more authors) (2024) B(OH)4− and CO32− do not compete for incorporation into aragonite in synthetic precipitations at pHtotal 8.20 and 8.41 but do compete at pHtotal 8.59. Geochimica et Cosmochimica Acta. pp. 39-52. ISSN 0016-7037

https://doi.org/10.1016/j.gca.2024.06.036

Geochimica et Cosmochimica Acta 379 (2024) 39–52

Contents lists available at ScienceDirect

Geochimica et Cosmochimica Acta

journal homepage: www.elsevier.com/locate/gca

$B(OH)_4^-$ and CO_3^{2-} do not compete for incorporation into aragonite in synthetic precipitations at pH_{total} 8.20 and 8.41 but do compete at pH_{total} 8.59

Cristina Castillo Alvarez [a,b], Kirsty Penkman [c], Roland Kröger [d], Adrian A. Finch [a], Matthieu Clog [e], Ed Hathorne [f], Nicola Allison [a,b,*]

[a] School of Earth and Environmental Sciences, University of St. Andrews, St Andrews KY16 9TS, UK
[b] Scottish Oceans Institute, University of St. Andrews, St Andrews KY16 8LB, UK
[c] Department of Chemistry, University of York, York YO10 5DD, UK
[d] Department of Physics, University of York, York, UK
[e] SUERC, University of Glasgow, UK
[f] GEOMAR Helmholtz Centre for Ocean Research Kiel, Kiel, Germany

ARTICLE INFO

Associate editor: Hao-Jia Ren

Keywords:
$CaCO_3$
$B(OH)_4^-$
Boron geochemistry
Coral
Biomineralisation
Aragonite precipitation
Amino acids

ABSTRACT

Coral skeletal B/Ca (effectively B/CO_3^{2-}), in combination with boron isotopic composition ($\delta^{11}B$), has been used to reconstruct the dissolved inorganic carbon chemistry of coral calcification media and to explore the biomineralisation process and its response to ocean acidification. This approach assumes that $B(OH)_4^-$, the B species incorporated into aragonite, competes with dissolved inorganic carbon species for inclusion in the mineral lattice. In this study we precipitated aragonite from seawater *in vitro* under conditions that simulate the compositions of the calcification media used to build tropical coral skeletons. To deconvolve the effects of pH and $[CO_3^{2-}]$ on boron incorporation we conducted multiple experiments at constant $[CO_3^{2-}]$ but variable pH and at constant pH but variable $[CO_3^{2-}]$, both in the absence and presence of common coral skeletal amino acids. Large changes in solution $[CO_3^{2-}]$, from < 400 to >1000 μmol kg^{-1}, or in precipitation rate, have no significant effect on aragonite B/Ca at pH_{total} of 8.20 and 8.41. A significant inverse relationship is observed between solution $[CO_3^{2-}]$ and aragonite B/Ca at $pH_{total} = 8.59$. Aragonite B/Ca is positively correlated with seawater pH across precipitations conducted at multiple pH but this relationship is driven by the effect of pH on the abundance of B $(OH)_4^-$ in seawater. Glutamic acid and glycine enhance the incorporation of B in aragonite but aspartic acid has no measurable effect. Normalising aragonite B/Ca to solution $[B(OH)_4^-]$ creates $K_D^{B(OH)4-}$ which do not vary significantly between pH treatments. This implies that $B(OH)_4^-$ and CO_3^{2-} do not compete with each other for inclusion in the aragonite lattice at pH_{total} 8.20 and 8.41. Only at high pH (8.59), when $[B(OH)_4^-]$ is high, do we observe evidence to suggest that the 2 anions compete to be incorporated into the lattice. These high pH conditions represent the uppermost limits reliably measured in the calcification media of tropical corals cultured under present day conditions, suggesting that skeletal B/Ca may not reflect the calcification media dissolved inorganic carbon chemistry in all modern day corals.

1. Introduction

Marine corals build aragonite skeletons that contribute substantially to the foundations of coral reefs, key structures in promoting biodiversity and fisheries, supporting tourism and providing coastal land protection (Spurgeon, 1992). Understanding the response of coral biomineralisation to current and future environmental change is critical to predicting the future of coral reefs. Coral skeletons are composite materials of aragonite and an organic matrix and their precipitation rates (calcification) are controlled by the $[CO_3^{2-}]$ and $[Ca^{2+}]$ of the fluid used to build the mineral (Burton and Walter, 1987; Morse et al., 2007) and by the presence of biomolecules (Mass et al., 2013; Falini et al., 2015; Kellock et al., 2020). Coral skeletal B/Ca is positively related to seawater B/CO_3^{2-} (Ram and Erez, 2023) and skeletal B/Ca has been used

* Corresponding author.
E-mail address: na9@st-andrews.ac.uk (N. Allison).

https://doi.org/10.1016/j.gca.2024.06.036
Received 30 July 2023; Accepted 27 June 2024
Available online 29 June 2024

as a tool to estimate the $[CO_3^{2-}]$ of the coral calcification media and to probe the response of biomineralisation to ocean acidification and climate change (e.g. Allison et al., 2014; McCulloch et al., 2017; Allison et al., 2018). In brief, $B(OH)_4^-$, one of the 2 predominant B species in seawater, is incorporated into the aragonite lattice, probably in place of CO_3^{2-} (Sen et al. 1994; Klochko et al., 2009; Noireaux et al. 2015). It has been assumed that $B(OH)_4^-$ competes with CO_3^{2-} or other dissolved inorganic carbon (DIC) species for inclusion in the lattice (Allison et al., 2014) and that coral aragonite B/Ca is thereby influenced by the concentration of the competing DIC species in the calcification media. For example, assuming $B(OH)_4^-$ competes with CO_3^{2-} then the aragonite distribution coefficient (K_D) can be defined as:

$$K_D^{B(OH)4-/CO32-} = \left(\left[B(OH)_4^-\right]/\left[CO_3^{2-}\right]\right)_{aragonite} / \left(\left[B(OH)_4^-\right]/\left[CO_3^{2-}\right]\right)_{calcificationmedia}$$

In this expression the ratio $([B(OH)_4^-]/[CO_3^{2-}])_{aragonite}$ is assumed to be the same as coral skeletal B/Ca (treating Ca^{2+} and CO_3^{2-} as equimolar in $CaCO_3$) and noting the B content of skeletal samples is measured relative to Ca after $CaCO_3$ dissolution. Boron speciation is pH dependent (Dickson 1990a) and $[B(OH)_4^-]_{calcification\ media}$ can be derived if the [B] and pH of the calcification media are known. In coral, calcification media pH are usually derived from the skeletal boron isotopic composition ($\delta^{11}B$, Rollion-Bard et al., 2003) and the [B] of the calcification media is assumed to be the same as local seawater assuming calcification media are ultimately derived from seawater.

Uncertainty surrounds the derivation of K_D in aragonite. Allison et al. (2014) estimated K_D for $B(OH)_4^-$ competing with various DIC species from $\delta^{11}B$ and B/Ca analysis of an aragonite cement in a fossil coral coupled with alkalinity measurements of coral skeleton pore fluids (Enmar et al., 2000). Holcomb et al. (2016) conducted synthetic aragonite precipitations in seawater and concluded that the B partitioning in aragonite may be influence by solution supersaturation (Ω) and/or mineral growth rate. They derived a K_D expression normalising aragonite B/Ca to solution $B(OH)_4^-/(CO_3^{2-})^{0.5}$, arguing that mineral charge balance was maintained by this ratio of anions. However coral skeletons also contain high concentrations of Na^+ (Mitsuguchi et al., 2010) and Na^+ and $B(OH)_4^-$ may substitute in pairs in aragonite to maintain charge balance (Henehan et al., 2022). Holcomb et al. (2016) also calculated Nernst partition coefficients which depended on media pH and Ω. Allison (2017) combined the Allison et al (2014) K_D estimates with the Holcomb et al. (2016) dataset and with additional data from precipitations of synthetic aragonite at low ionic strength by Mavromatis et al. (2015). Allison (2017) calculated K_D by normalising aragonite B/Ca to solution $B(OH)_4^-/CO_3^{2-}$, $B(OH)_4^-/HCO_3^-$ and $B(OH)_4^-/(CO_3^{2-}+HCO_3^-)$ and concluded that all these K_D were positively related to the ratio of the concentrations of precipitating ions i.e. Ca^{2+} and either CO_3^{2-}, HCO_3^- or both, in solution. However, observed patterns between coral skeletal B/Ca and $\delta^{11}B$ derived coral calcification media pH could not be generated using these expressions (Allison, 2017).

pH and solution $[CO_3^{2-}]$ covary in both the Mavromatis et al. (2015) and Holcomb et al. (2016) studies (Fig. 1.). This complicates the identification of relationships between aragonite B/Ca and solution DIC as boron speciation is pH dependent i.e. both $B(OH)_4^-$ and CO_3^{2-} are more abundant at high pH. In the present study we seek to deconvolve the effects of pH and $[CO_3^{2-}]$ on B incorporation in aragonite. We report the B/Ca of a series of synthetic aragonites precipitated from artificial seawaters with Ω altered to reflect the range inferred for coral calcification media (Castillo Alvarez et al., 2024). pH and $[CO_3^{2-}]$ co-vary in seawater at constant seawater pCO_2 and to separate the influence of each of these parameters on aragonite B/Ca we performed experiments under different CO_2 atmospheres i.e. varying pH at constant $[CO_3^{2-}]$ and varying $[CO_3^{2-}]$ at constant pH.

The DIC chemistry of tropical coral calcification media has been measured directly using pH sensitive SNARF dyes (e.g. Venn et al., 2011) and microelectrodes (e.g. Al-Horani et al., 2003). SNARF fluorescent dye and microelectrode measurements at the growth edges of coral microcolonies suggest that the pH_{total} of the extracellular calcification media of corals cultured at present day pCO_2 is ~8.3 to ~8.6 (Venn et al., 2011, 2013; Sevilgen et al, 2019) while $[CO_3^{2-}]$ is ~400–870 μmol kg^{-1} (Sevilgen et al., 2019). In combination, these estimates suggest the calcification media has $\Omega_{aragonite} \approx 12$ (Sevilgen et al., 2019). Microelectrode measurements within coral colonies suggest that calcification media parameters may be as high as pH_{total} =10.0 with $[CO_3^{2-}]$ = 1400 μmol kg^{-1}, yielding $\Omega_{aragonite} \approx 22$ (Cai et al., 2016). However the microsensor position can not be visualised in these within-colony studies and a comparison of growth edge and within-colony estimates suggests that within-colony microsensor measurements do not accurately record calcification media DIC chemistry (Sevilgen et al., 2019). Calcification media pH has also been inferred from $\delta^{11}B$ analysis of coral skeletons (e.g. Rollion-Bard et al., 2003). However a recent study comparing SNARF and $\delta^{11}B$ estimates of calcification media pH suggests that $\delta^{11}B$ yields media pH which are ~0.4 units higher that by SNARF although the origin of this effect is unclear (Allison et al., 2023).

In the present study we use pH_{total} = 8.20–8.59 and $[CO_3^{2-}]$ = ~250–1150 μmol kg^{-1}, yielding $\Omega_{aragonite}$ = 4–18. This range includes both the calcification media conditions likely to occur in present day corals and in corals cultured under ocean acidification conditions when calcification media pH is reported to decrease (Venn et al., 2013, 2019; Holcomb et al., 2014). Coral skeletons contain ~2.5% hydrated organic materials by mass (Cuif et al., 2004) and these biomolecules and their constituents can influence both $CaCO_3$ precipitation (Falini et al., 2015,

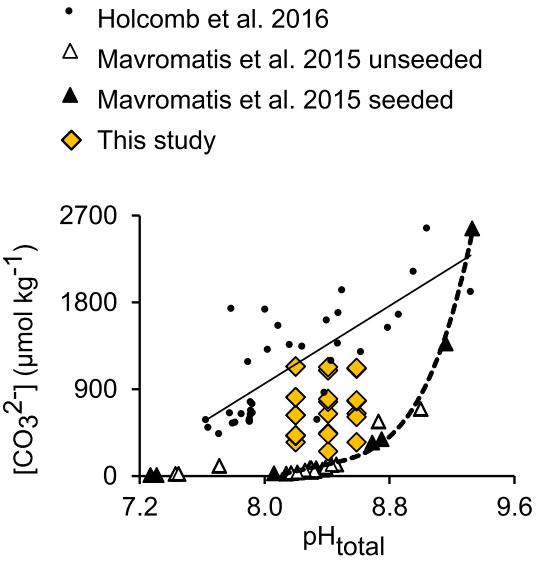

Fig. 1. Summary of the solution conditions used in the present study and in previous studies of boron partitioning in aragonite. Significant positive correlations occurred between solution pH and $[CO_3^{2-}]$ in both the Holcomb et al., 2016 (linear regression in solid line, $r^2 = 0.59$) and Mavromatis et al., 2015 (polynomial regression in dotted line, $r^2 = 0.98$) studies.

Kellock et al., 2020, 2022) and $CaCO_3$ chemistry (Mavromatis et al., 2017). We conduct precipitations in the presence of the three most common coral skeletal amino acids (aspartic acid, glutamic acid and glycine, Kellock et al., 2020) to define their role in influencing aragonite B/Ca.

2. Methods

2.1. Aragonite precipitations

The precipitation of the aragonite samples analysed here is reported in Castillo Alvarez et al., 2024. All consumables were acid cleaned (1.0 M trace element grade HCl) prior to use and rinsed with type 1 water (18.2 MΩ cm^{-1}). Aragonite was precipitated from artificial seawater at 25°C over a range of pH and [CO_3^{2-}] conditions (Fig. 1) using the constant composition method (Beck et al., 2013, Kellock et al., 2020, 2022) i.e. maintaining aqueous [Ca^{2+}] and [CO_3^{2-}] during the precipitation. We utilised pH and DIC conditions that are representative of the coral calcification media as measured by Sevilgen et al. 2019.

2 batches of seawater were prepared for precipitations using the recipe of Millero (2013) and resulting in salinity of 35 and total alkalinity of 2192 or 2232 μmol kg^{-1} (batches 1 and 2 respectively). The total alkalinity of a subset (10 L) of the first batch was reduced by the addition of 2M trace element grade HCl to produce a seawater with lower DIC (after CO_2 outgassed) for experiments at low [DIC] (<2000 μmol kg^{-1}). Seawater was kept at 25°C and equilibrated with ~410 ppm CO_2 air by bubbling with air drawn from outside the building. For each precipitation, 340 mL seawater was filtered through a 0.2 μm polyether sulfone filter, poured into a high density polyethylene beaker and capped with an ethylene tetrafluoroethylene lid with ports through which a pH/temperature sensor, a propeller stirrer, a gas tube and 2 titrant dosing tubes were inserted. The vessel was immersed in a water bath at 25°C. The [DIC] and pH of the seawater were manipulated to predetermined values by the addition of trace element grade 0.6M Na_2CO_3 and 2M HCl or 2M NaOH. The gas tube into the vessel supplied air with the [CO_2] adjusted to be in equilibrium with the manipulated seawater. Ambient pCO_2 air streams (410 ppm CO_2) used air sourced from outside the building and filtered and warmed before use. Above ambient CO_2, airstreams were produced by combining ambient air with high purity CO_2 using high precision mass flow controllers (SmartTrak 50 Series, Sierra USA). Below ambient CO_2 airstreams were produced by flowing ambient air through NaOH pellets to remove CO_2 and then combining this with high purity CO_2 as before. Airstream [CO_2] was determined using an infrared CO_2 analyser (WMA04, PP systems, USA)

The pH of the reaction solution was monitored using a combined pH/temperature sensor (Metrohm Aquatrode PT1000) connected to a Metrohm Titrando 902 titrator. The sensor was calibrated weekly with fresh NIST (National Institute of Standards and Technology) buffers. pH was measured on the NBS (National Bureau of Standards) scale but was converted to the total scale for comparison to previous reports in the literature. pH_{total} is 0.136–0.137 units lower than pH_{NBS} over the pH range used here. pH drift between weeks was ≤0.004 pH units. At the start of each experiment, 200 ± 1 mg of an aragonite seed with surface area of 4.27 ± 0.11 m^2/g (1σ, n=3 as analysed by the Brunauer–Emmett–Teller technique) was added to the manipulated seawater to provide a surface for aragonite growth. The seed was produced by cleaning a modern coral skeleton with sodium hypochlorite, rinsing it repeatedly and then grinding it in an agate ball mill. This seed provides a surface for growth that is analogous to a coral skeleton. Aragonite precipitation onto the seed, decreased the pH of the solution in the reaction vessel and triggered the automatic addition of 0.45M Na_2CO_3 and 0.45 M $CaCl_2 + SrCl_2$ in a 99:1 ratio, to restore pH (Na_2CO_3) and to replace the ions used in precipitation (both titrants). Aragonite precipitation proceeded until 6.7 mL of each titrant was dosed, indicating that 300 mg of aragonite was precipitated during the experiment. At the end of each titration, solids (combining seed and precipitate) were collected by filtration onto acid cleaned 0.2 μm polyether sulfone filters, rinsed with type 1 water and then with trace element clean grade ethanol. Minor amounts of solids adhered to the pH sensor and dosing tubes and these were not recovered. Samples were dried at room temperature and stored in a desiccator prior to analysis.

Seawater [DIC] was measured at the start and end of each experiment using a CO_2 differential, non-dispersive, infrared gas analyser (Apollo SciTech; AS-C3) calibrated with a certified reference material (CRM 194, Scripps Institution of Oceanography). The DIC parameters of each experiment were calculated from the manipulated seawater pH and [DIC] using CO_2 Sys v2.1 (Pierrot et al., 2006) with the equilibrium constants for carbonic acid and $KHSO_4$ from Lueker et al. (2000) and Dickson (1990b) respectively and seawater [B] from Lee et al. (2010). $\Omega_{aragonite}$ was calculated using solution [CO_3^{2-}], solution [Ca^{2+}], as measured in section 2.2 and the solubility product (K_{sp}) of aragonite at 25°C and 1 atmosphere (Mucci, 1983). Aragonite precipitation rates were calculated by normalising titrant dosing rates to seed surface area (Kellock et al., 2022).

Titrations with no amino acid were conducted at $pH_{total} = 8.20$, 8.41 and 8.59 and at $\Omega_{aragonite} = \sim 4$, 7, 10, 13 and 18. Aspartic acid, glutamic acid and glycine, where used, were sourced from Sigma-Aldrich (purity ≥99%), dissolved in seawater and added to the titration vessel to achieve the required concentration before the addition of Na_2CO_3. Titrations were conducted with 2 mM of each amino acid over the same range of pH and Ω values as used in the titrations with no acid, with the exception that precipitations at Ω=4 were not perfomed. Each set of conditions were replicated 3 or 4 times and 1 – 3 of these replicates were analysed for boron geochemistry. Finally the effect of 0.2, 1, 2, 3 and 5 mM of each amino acid at $pH_{total} = 8.34$ and $\Omega_{aragonite} \approx 13$ on aragonite B/Ca was explored. These final experiments were not replicated.

2.2. B/Ca of seawaters and aragonites

The [B] and [Ca] were measured for each batch of seawater, at the start of select experiments (to confirm that seawater B/Ca was not significantly affected by the addition of reagents (e.g. HCl, NaOH or amino acids) and at the end of all precipitations. Seawaters were filtered through 0.2 μm polyether sulfone filters, stored in high density polyethylene tubes and acidified to pH 2 with 69% trace element clean grade HNO_3. Prior to analysis, samples were diluted 1:10 with 2% HNO_3 (including yttrium as an internal standard) and measured using a Varian ICP-OES at GEOMAR. Elemental wave lengths K 766.491, Mn 257.610, Li 670.783, B 249.772, Ba 455.403, Na 330.237, Si 251.611, Fe 238.204, Na 568.821, Si 288.158, Ba 493.408, Ca 370.602, Ca 318.127, K 769.897, Mg 277.983, Mg 285.213, Sr 215.283, Sr 460.733, Sr 407.771, Al 167.019, Al 396.152, were monitored and counts calibrated using standards mixed from single element solutions. International Association for the Physical Sciences of the Oceans (IAPSO) standard seawater was repeatedly diluted as for the samples and measured. Seawaters were measured in 2 batches, with seawaters from the experiments with no amino acids analysed in the first batch and all the other seawaters analysed in the second batch. The mean [B] and [Ca] obtained for the IAPSO seawater were 0.443 ± 0.004 mM and 10.49 ± 0.02 mM, respectively (2 standard deviations, n = 6) for batch 1 and 0.436 ± 0.017 mM and 10.25 ± 0.14 mM (n=10) respectively for batch 2. Coefficients of variation for these repeat analyses are <2% for B and ≤0.7% for Ca within each batch and [B] and [Ca] agree within 2% between batches. Procedural blanks, consisting of type 1 water filtered, stored and acidified as for seawater samples, had [B] and [Ca] of 0.004 mM and 0.00 mM respectively which in each case were <1 % of seawater values.

Solids and samples of the starting seed were dissolved stepwise with distilled 0.1 M HCl in acid-cleaned polypropylene micro-centrifuge tubes, centrifuged at 13 x 10^3 rpm (using an Eppendorf microfuge), and then transferred to clean micro-centrifuge tubes leaving a small volume of solution in the dissolution tube. The sample solution was diluted with 2% HNO_3 (with Sc as an internal standard) and B/Ca ratios

were measured by ICP-MS (Agilent 7500ce) alongside a standard solution mixed from single element solutions (Inorganic Ventures) to concentrations typically found in coral samples. The instrument was calibrated following the method of Rosenthal et al. (1999). The Ca concentration of the measured samples was within the range of calibration standards and no matrix effect was observed for this range. The mean values for 2 reference materials, JCp-1 (Hathorne et al., 2013) and NIST RM 8301 (Stewart et al., 2021), analysed in the same runs, are presented in Table S1. B/Ca of replicate analyses of these reference materials at the typical B/Ca observed in the synthetic aragonites (i.e. for JCp-1 and for NIST RM 8301 diluted to replicate a coral aragonite) agree within 3–7% (2 standard deviations, 2s). The B/Ca of the synthetic aragonites and seed were measured and the B/Ca of the aragonite precipitated *in vitro* was determined by correcting for the seed composition assuming the seed comprised 40% of the total solid mass.

2.3. Precipitate characterisation

Raman spectroscopy confirmed that all precipitates were aragonite (Castillo Alvarez et al., 2024). Selected precipitates were viewed uncoated by scanning electron microscope (SEM, JEOL 7800F Prime) using a beam current of 0.04nA and an accelerating voltage of 2 keV.

3. Results

3.1. Aragonite B/Ca in precipitates with no added amino acids

Seawater [B] and [Ca] at the start of titrations agree with the [B] and [Ca] of the batch seawater within 2%, indicating that the manipulation of seawater DIC chemistry and addition of amino acids, if used, has little effect on seawater element chemistry. We considered the errors likely to influence our experiments. Seawater DIC typically varied by <5% over precipitations while seawater [B] and [Ca] decreased by 4% and 8% respectively, on average and by 16% and 18% at most. The B/Ca of the aragonite precipitated during the titrations varies from 0.311 to 0.768 mmol mol^{-1} which is a much broader range (247%) than can be accounted for by changes in solution [B] (≤16%). The mass of the starting seed was 200 ± 1 mg (an error of 0.5% which we consider insignificant). B/Ca of the seed used for the precipitations ranged from 412 to 447 μmol mol^{-1} probably because coral skeletons are heterogeneous with respect to B/Ca (Sinclair, 2005). The standard deviation of duplicate analyses of the seed yields a B/Ca standard deviation of ± 25 μmol mol^{-1}. This is likely to be an overestimate of variations in seed B/Ca between precipitations as 200 mg of seed were used for each precipitation (averaging B/Ca over a larger mass of seed) while only ~20 mg of each aliquot of seed was sent for B analysis. The seed contributes 40% of the mass of the solid collected at the end of the precipitation so variations in seed B/Ca of this magnitude could influence the final B/Ca by ± 10 μmol mol^{-1}. Again, we consider this error to be small in comparison with the total range of B/Ca observed in the final solids (359–632 μmol mol^{-1}). Assuming that errors are random we estimate a total error for aragonite B/Ca estimates of 20 μmol mol^{-1} by compounding the precision of B/Ca of the solid (≤17 μmol mol^{-1}, 1s), the error associated with variation in B/Ca of the starting seed (10 μmol mol^{-1}, 1s) and the potential influence of variations in the mass of the seed (2 μmol mol^{-1}, assuming that the seed has B/Ca = 429 μmol mol^{-1} and varies by up to 0.5% between titrations).

In precipitations conducted with no amino acids, we observe a strong positive linear correlation between pH and aragonite B/Ca (Fig. 2a, supplementary data Table S2). To explore if [CO_3^{2-}] influences this relationship, we divide the dataset into low (<600 μmol kg^{-1}), mid (600–900 μmol kg^{-1}) and high (>1000 μmol kg^{-1}) CO_3^{2-} concentrations. Strong positive linear correlations are observed within each of these ranges but one-way ANCOVA indicates that this relationship is significantly different at high [CO_3^{2-}] compared to mid and low [CO_3^{2-}], with aragonite B/Ca offset to lower values at high [CO_3^{2-}] after correcting for pH variance (Table S2).

Aragonite B/Ca is not significantly related to seawater [CO_3^{2-}] or precipitation rate over the whole dataset (Fig. 2b, Fig. S1, Table S2). Within each pH treatment, aragonite B/Ca and both seawater [CO_3^{2-}] and precipitation rate are not significantly related at pH 8.20 and 8.41 but are significantly inversely related at 8.59 (Table S2). In these experiments, seawater [CO_3^{2-}] is strongly positively correlated (r^2=0.99) with aragonite precipitation rate (Castillo Alvarez et al., 2024) so aragonite B/Ca exhibits similar distribution patterns when compared to [CO_3^{2-}] or precipitation rate. [Ca^{2+}] was approximately constant across the precipitations so [CO_3^{2-}] is the main control on precipitation rate in these experiments.

3.2. Boron incorporation in relation to solution chemistry

To explore controls on B incorporation in aragonite we plot aragonite B/Ca as a function of B/DIC (as in Uchikawa et al., 2015), and of B$(OH)_4^-$/CO_3^{2-}, B$(OH)_4^-$/HCO_3^- and B$(OH)_4^-$/$(CO_3^{2-})^{0.5}$ (as in Holcomb et al., 2016), (Fig. 3). Coefficients of determination and p values for linear regression analyses of the relationships between aragonite B/Ca and

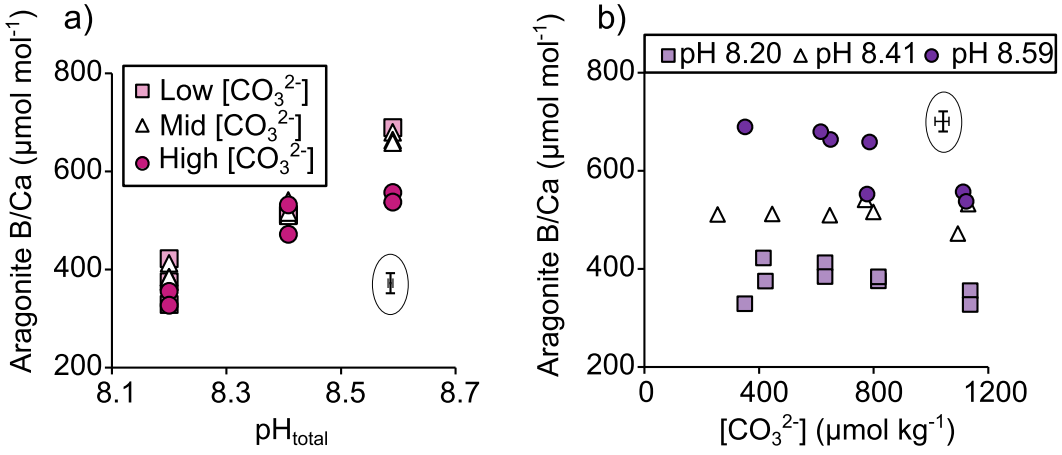

Fig. 2. B/Ca of aragonite precipitated in the absence of amino acids as a function of a) pH (total scale) and b) seawater [CO_3^{2-}]. In a) Low CO_3^{2-} = <600 μmol kg^{-1}, mid CO_3^{2-} = 600–900 μmol kg^{-1} and high CO_3^{2-}= >1000 μmol kg^{-1}. Typical errors in B/Ca, pH and [CO_3] are represented by the floating error bars which are ringed for clarity. Compounding B/Ca error is discussed in section 3.1. pH uncertainty is estimated from the maximum drift in sensor pH observed over a week (as ± 0.002 units) and [CO_3] uncertainty is estimated by compounding the typical change in DIC over the course of a titration (<±2.5 %) with the pH error to yield a [CO_3] uncertainty of ± 2.5 %.

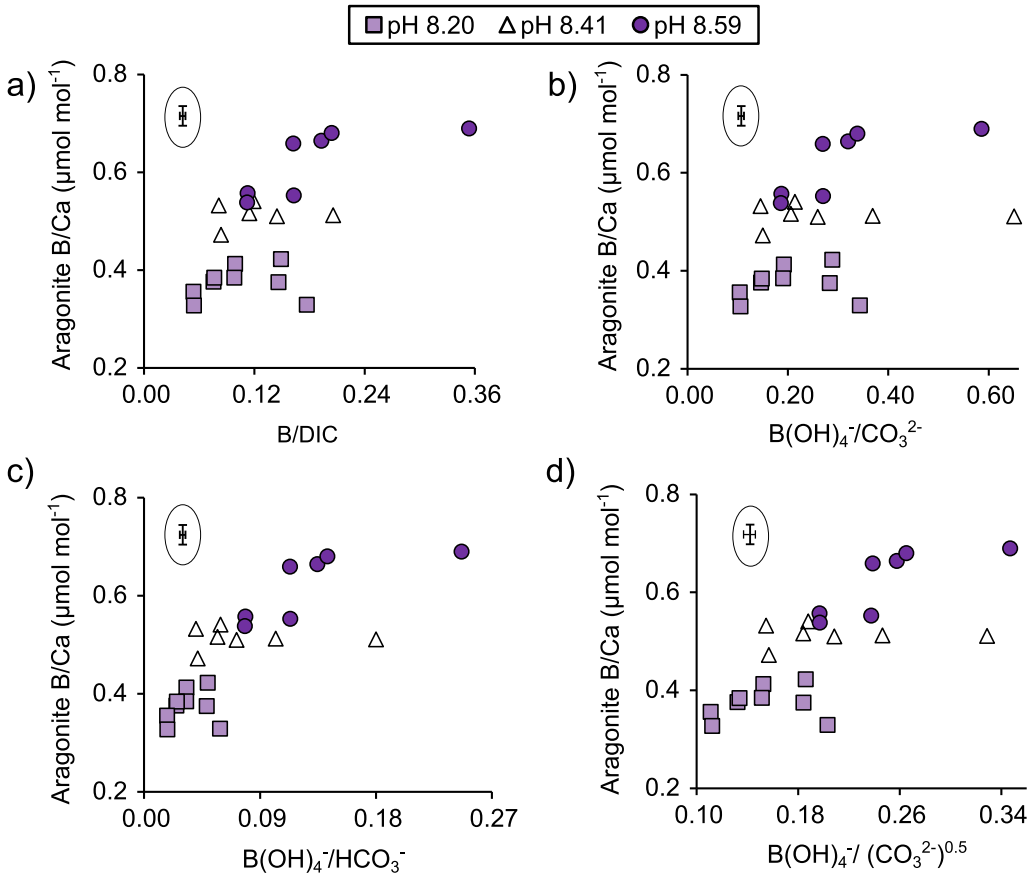

Fig. 3. B/Ca of aragonite precipitated in the absence of amino acids as a function of solution a) B/DIC, b) $B(OH)_4^-/CO_3^{2-}$, c) $B(OH)_4^-/HCO_3^-$ and d) $B(OH)_4^-/(CO_3^{2-})^{0.5}$. Typical errors in B/Ca and solution chemistry are represented by the floating error bars which are ringed for clarity. Compounding the solid B/Ca error is discussed in section 3.1. Solution B/DIC species uncertainty is estimated by compounding the error in solution [B] measurement (±0.004 mM) and the typical DIC error over a titration (±2.5 %). Solution $B(OH)_4^-/CO_3^{2-}$, $B(OH)_4^-/HCO_3^-$ and $B(OH)_4^-/(CO_3^{2-})^{0.5}$ uncertainties are calculated by compounding the error in solution [B] measurement (0.9 %) with the pH error (±0.002 pH units, which influences $[B(OH)_4^-]$ by up to 0.6 %) and the typical change in [DIC] (±2.5 %).

Table 1
Coefficients of determination and p values for linear regression analyses of the relationships between aragonite B/Ca and solution parameters. Values are shown for the whole dataset and for each pH individually. p values ≤ 0.05 are highlighted in bold.

Solution parameter	All pH		pH 8.20		pH 8.41		pH 8.59	
	r^2	p	r^2	P	r^2	p	r^2	p
$B(OH)_4^-/CO_3^{2-}$	0.20	**0.024**	0.060	0.50	0.012	0.80	0.54	0.059
$B(OH)_4^-/(CO_3^{2-})^{0.5}$	0.55	**2.3×10^{-5}**	0.094	0.39	0.024	0.72	0.61	**0.038**
$B(OH)_4^-/HCO_3^-$	0.61	**4.2×10^{-6}**	0.060	0.50	0.012	0.80	0.54	0.059
$B(OH)_4^-$/DIC	0.55	**2.2×10^{-5}**	0.060	0.50	0.012	0.80	0.54	0.059
B/DIC	0.30	**0.0050**	0.060	0.50	0.012	0.80	0.54	0.059

these solution parameters are detailed in Table 1, alongside the relationship between aragonite B/Ca and $B(OH)_4^-$/DIC (not shown in figure form).

Significant positive relationships are observed between aragonite B/Ca and B/DIC, $B(OH)_4^-$/DIC, $B(OH)_4^-/CO_3^{2-}$, $B(OH)_4^-/HCO_3^-$ and $B(OH)_4^-/(CO_3^{2-})^{0.5}$ when all pH treatments are combined. Relationships between aragonite B/Ca and B/DIC, $B(OH)_4^-$/DIC, $B(OH)_4^-/CO_3^{2-}$, $B(OH)_4^-/HCO_3^-$ and $B(OH)_4^-/(CO_3^{2-})^{0.5}$ within single pH treatments are weak ($r^2<0.1$) at pH 8.20 and 8.41 but are stronger ($r^2>0.5$) at pH 8.59 (Table 1). Numbers of precipitations within each pH treatment are small (n = 7 to 10) which limits statistical power but p values at pH 8.20 and 8.41 are high (≥0.60) and at pH 8.59 are low (≤0.059). Coefficients of determination and p values for each pH treatment are the same, regardless of whether B/DIC, $B(OH)_4^-$/DIC, $B(OH)_4^-/CO_3^{2-}$ or $B(OH)_4^-/HCO_3$ is the x variable. This is because [B] and $[B(OH)_4^-]$ are essentially constant within each pH treatment, $[CO_3^{2-}]$ and $[HCO_3^-]$ are directly proportional at constant pH and combined they make up the vast majority of DIC at pH 8.2 and above i.e. CO_2 is <0.5% of DIC above this pH.

3.3. $K_D^{B(OH)4-}$ in precipitations with no amino acids

Our data demonstrate that increases in inorganic carbon solutes (either as DIC, $[CO_3^{2-}]$, $[HCO_3^-]$ or $[CO_3^{2-}]^{0.5}$) have no significant effect on boron incorporation at pH 8.20 and 8.41 and an inverse effect at pH 8.59. To visualise the data with no influence of solution DIC, $[CO_3^{2-}]$, $[HCO_3^-]$ or $[CO_3^{2-}]^{0.5}$ on boron incorporation, we calculate boron aragonite distribution coefficients as:

$K_D^{B(OH)4-} = [B]_{solid} / [B(OH)_4^-]_{solution}$, where both concentrations are in mol kg^{-1}.

$[B]_{solid}$ is calculated from measured precipitate B/Ca using the molecular mass of pure $CaCO_3$ of 100 g. $B(OH)_{4solution}^-$ is estimated from the average measured [B] of seawater (in mol kg^{-1}) using K^*_B (Dickson

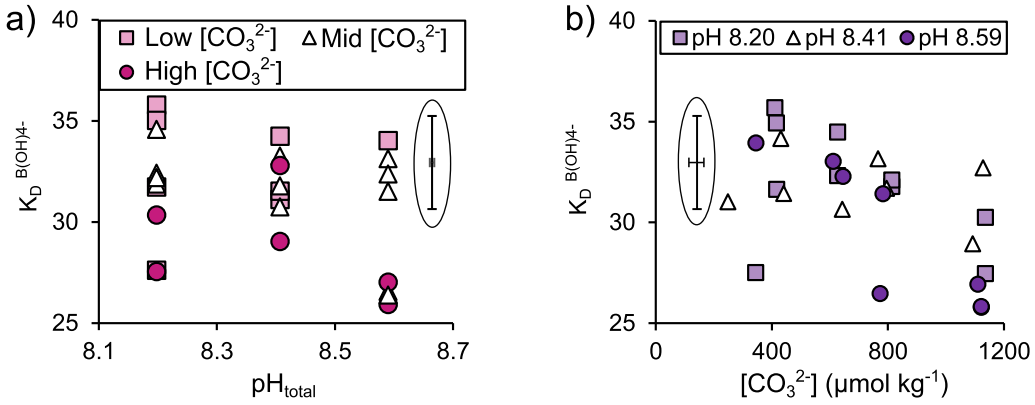

Fig. 4. K_D $^{B(OH)4-}$ in experiments with no amino acids as a function of pH and $[CO_3^{2-}]$. Typical errors in K_D, pH and $[CO_3^{2-}]$ are represented by the floating error bars which are ringed for clarity. Errors in K_D are estimated by compounding the errors in solution $[B(OH)_4^-]$ (typically 5.1 % see legend for Fig. 3) and solid $[B(OH)_4^-]$ (20 µmol mol^{-1}, see section 3.1). Errors in pH and $[CO_3^{2-}]$ are defined in the legend to Fig. 2.

Table 2
Summary of statistical tests of data in Figs. 4 and 6. The first half of the table presents coefficients of determination (r^2) and p values for linear relationships between K_D $^{B(OH)4-}$ and pH and CO_3^{2-} across precipitations made with and without amino acids. The second half of the table presents ANCOVA p values comparing relationships between K_D and pH or $[CO_3^{2-}]$ for precipitations conducted with and without amino acids. ANCOVA tests for equal means (after correcting for variance) and equal slopes between populations. p values ≤ 0.05 are highlighted in bold.

Statistical test		
Linear regression analysis	**r^2**	**p value**
K_D versus pH (all $[CO_3^{2-}]$)		
With no amino acid (Fig. 6a)	$r^2 = 0.068$	$p = 0.21$
With 2 mM aspartic acid (Fig. 6b)	$r^2 = 0.19$	**$p = 0.039$**
With 2 mM glutamic acid (Fig. 6c)	$r^2 = 0.13$	$p = 0.099$
With 2 mM glycine (Fig. 6d)	$r^2 = 0.34$	**$p = 0.0041$**
K_D versus CO_3^{2-}		
With no amino acid (all pH, Fig. 4b)	$r^2 = 0.27$	**$p = 0.0079$**
With no amino acid (pH 8.59 only, Fig. 4b)	$r^2 = 0.74$	**$p = 0.012$**
With 2 mM aspartic acid (all pH, Fig. S2b)	$r^2 = 0.12$	$p = 0.10$
With 2 mM glutamic acid (all pH, Fig. S2c)	$r^2 = 0.024$	$p = 0.49$
With 2 mM glycine (all pH, Fig. S2d)	$r^2 = 3.6 \times 10^{-3}$	$p = 0.79$
One-way ANCOVA	**p (equal means)**	**p (equal slopes)**
K_D versus pH (all $[CO_3^{2-}]$)		
Aspartic acid compared to no amino acid	0.40	0.22
Glutamic acid compared to no amino acid	**3.5×10^{-5}**	0.41
Glycine compared to no amino acid	**3.6×10^{-9}**	0.11
K_D versus $[CO_3^{2-}]$		
Aspartic acid compared to no amino acid	0.68	0.68
Glutamic acid compared to no amino acid	**8.1×10^{-5}**	0.060
Glycine compared to no amino acid	**2.6×10^{-8}**	0.24

1990a), calculated from the measured precipitation temperature and salinity. This effectively normalises aragonite B/Ca to the influence of the pH effect on $B(OH)_4^-$ speciation in solution but assumes that changes in DIC, $[CO_3^{2-}]$, $[HCO_3^-]$ or $[CO_3^{2-}]^{0.5}$ do not affect B incorporation in aragonite.

K_D $^{B(OH)4-}$ are broadly comparable between all precipitations (Fig. 4) and are not significantly related to pH either over all $[CO_3^{2-}]$ (Table 2) or when $[CO_3^{2-}]$ are divided into low (>600 µmol kg^{-1}), mid (600–1000 µmol kg^{-1}) or high (>1000 µmol kg^{-1}) groups (Table S3). $[CO_3^{2-}]$ and K_D are not significantly related at pH 8.20 or 8.41 but are significantly inversely related at pH 8.59 (Table S3) yielding a weak inverse relationship (r^2=0.27) between $[CO_3^{2-}]$ and K_D over the entire dataset (Table 2). The K_D versus pH relationship is offset to lower K_D at high $[CO_3^{2-}]$ compared to both mid and low $[CO_3^{2-}]$ (Table S3). There are no significant differences in relationships between K_D and $[CO_3^{2-}]$ at any pH (one way ANCOVA) with the exception that the slope between $[CO_3^{2-}]$ and K_D is significantly different at high $[CO_3^{2-}]$ compared to mid $[CO_3^{2-}]$ (Table S3).

3.4. Effect of amino acids on K_D $^{B(OH)4-}$

The addition of free aspartic acid, glutamic acid and glycine reduces aragonite precipitation rates (by up to >75% in the case of aspartic acid, Fig. 5a). Both glycine and glutamic acid exhibit positive linear correlations between K_D $^{B(OH)4-}$ and amino acid concentration and this relationship is significant for glycine (Fig. 5b, Table 3). The increase in K_D at the highest glycine and glutamic acid concentrations compared to the precipitation with no amino acids is relatively small i.e.10% and 7% respectively.

K_D $^{B(OH)4-}$ are calculated for all precipitations conducted with 2 mM aspartic acid, glutamic acid or glycine and plotted as a function of pH (Fig. 6) and $[CO_3^{2-}]$ (Fig. S2). There are significant inverse linear relationships between K_D and pH with aspartic acid (Fig. 6b, Table 2) and with glycine (Fig. 6d) across all pH treatments, although these relationships are not significant with no amino acid or with glutamic acid (Fig. 6 a,c). Relationships between pH and K_D $^{B(OH)4-}$ are significantly different in the presence of glycine or glutamic acid compared to

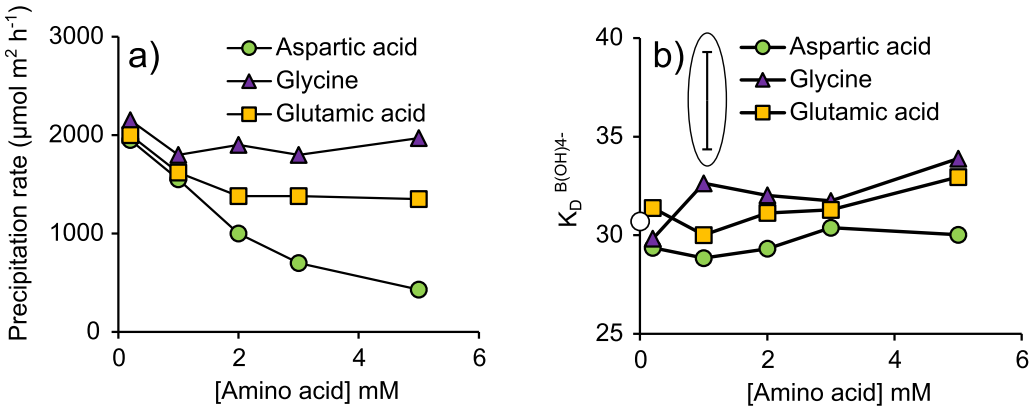

Fig. 5. Effect of variable concentrations of amino acids on a) aragonite precipitation rates (replotted from Castillo Alvarez et al., 2024) and b) K_D $^{B(OH)4-}$ at $[CO_3^{2-}]$ = 822 µmol kg^{-1}, pH total = 8.337. The typical errors in K_D is defined as in the legend to Fig. 4 and represented by the floating error bar which is ringed for clarity in b). Titrations were not replicated and no error is estimated for precipitation rate.

Table 3
Coefficients of determination (r^2) and p values for linear relationships between $K_D^{B(OH)4-}$ and amino acid concentration for each amino acid. p values ≤ 0.05 are highlighted in bold.

	r^2	p value
Aspartic acid	$r^2 = 0.03$	p = 0.74
Glutamic acid	$r^2 = 0.60$	p = 0.069
Glycine	$r^2 = 0.67$	**p = 0.047**

precipitations with no amino acid (Fig. 6, Table 2). To explore if $[CO_3^{2-}]$ influenced the K_D versus pH relationship, we split the dataset for each amino acid into low (<600 µmol kg^{-1}), mid (600–1000 µmol kg^{-1}) and high (>1000 µmol kg^{-1}) CO_3^{2-} concentrations and used ANCOVA to test for differences in the relationships between pH and K_D between $[CO_3^{2-}]$ groups (Table S4). We observe no significant differences between these $[CO_3^{2-}]$ groups for each amino acid. $[CO_3^{2-}]$ has no significant effect on K_D in the presence of 2 mM of any of the amino acids either across all pH treatments combined (Table 2) or within a single pH treatment (Table S5). K_D in the presence of aspartic acid are not significantly

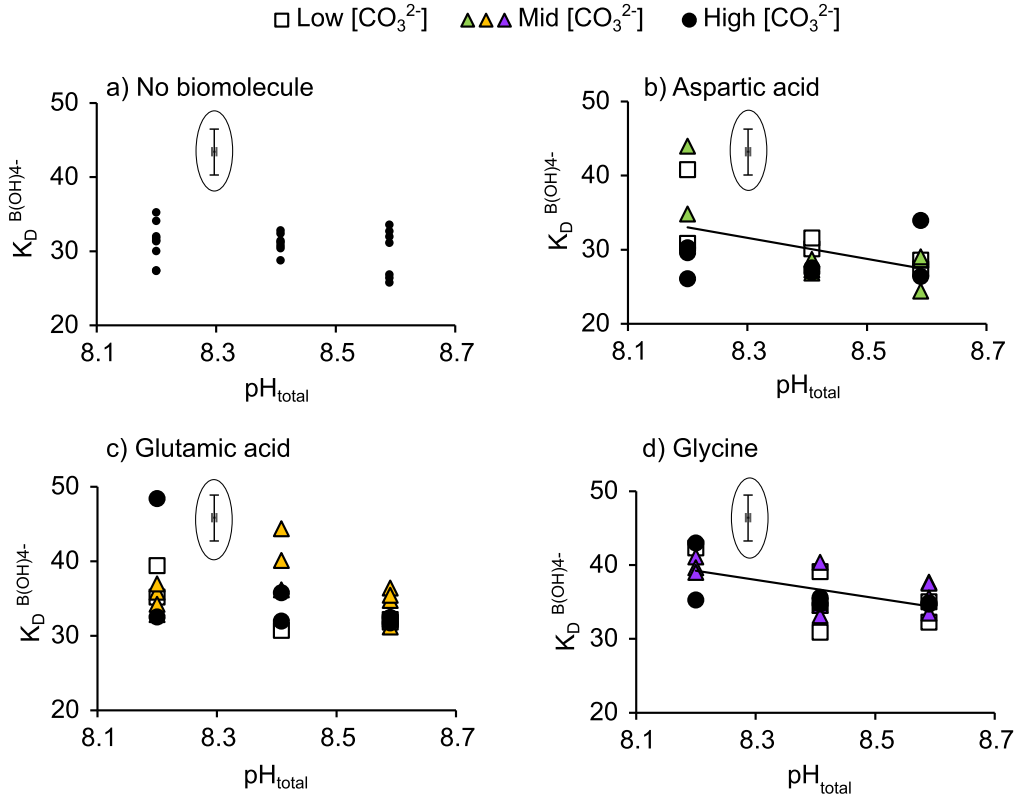

Fig. 6. $K_D^{B(OH)4-}$ at the DIC conditions in Fig. 1a with a) no amino acid (a repeat of the data from Fig. 3a), b) 2 mM aspartic acid, c) 2 mM glutamic acid and d) 2 mM glycine. Regressions are shown where relationships between pH and K_D are significant across the whole dataset (Table 2). To highlight variations between precipitations conducted at different $[CO_3^{2-}]$, data for b-d) are split into groups as for Fig. 1. The typical errors in K_D and pH are defined as in the legends to Fig. 4 and Fig. 2 respectively and represented by the floating error bars which are ringed for clarity.

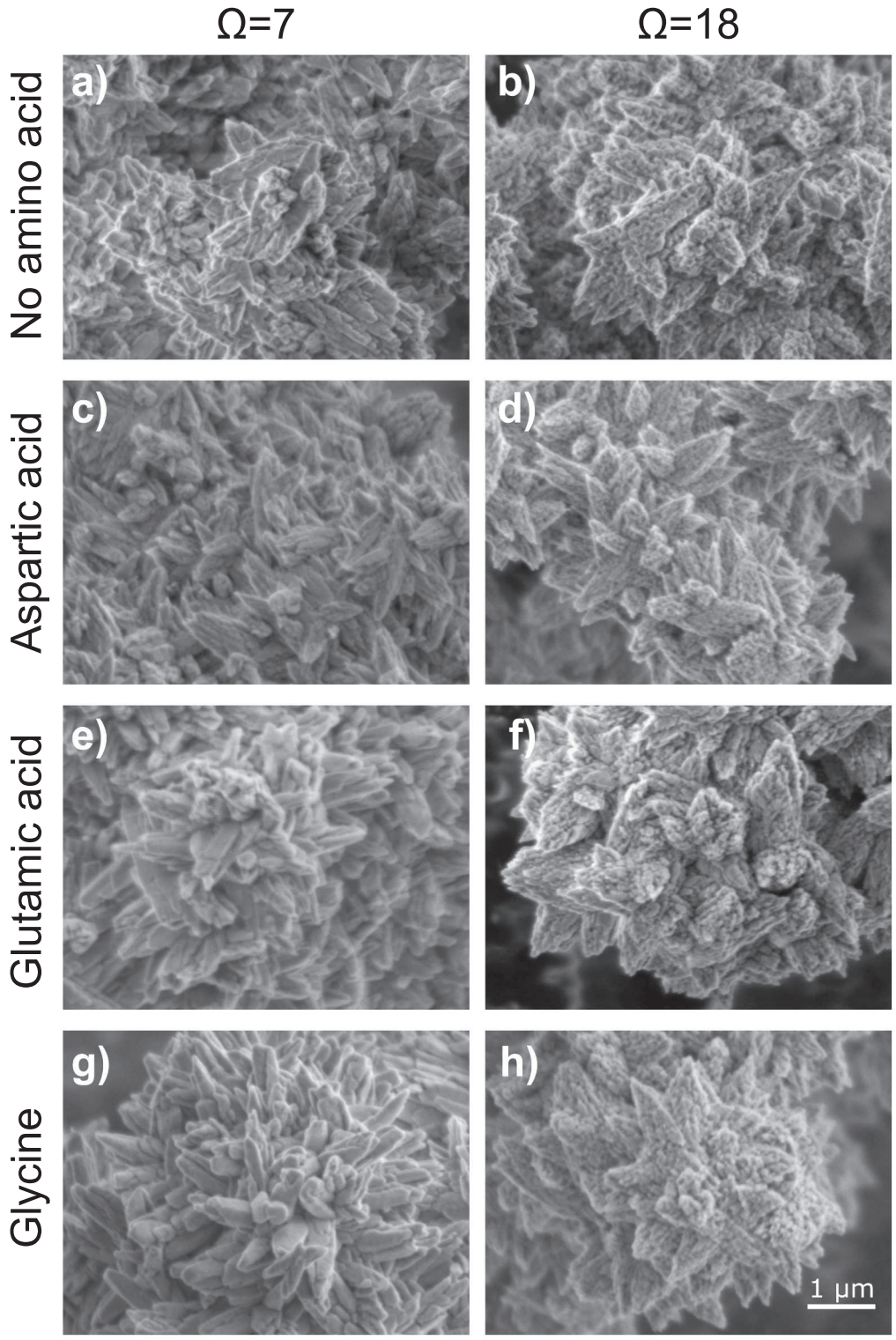

Fig. 7. SEM images of aragonites precipitated at Ω = 7 and 18 (both at pH_{total} 8.20) with a) and b) no amino acid, c) and d) 2 mM of aspartic acid, e) and f) 2 mM glutamic acid and g) and h) 2 mM glycine.

different compared to those in experiments with no amino acid either as a function of pH or $[CO_3^{2-}]$ (Table 2).

3.5. Morphology of synthetic aragonites

We present typical scanning electron micrographs for aragonites precipitated at Ω=7 and 18 (both at pH_{total} 8.20) and with no amino acid or in the presence of 2 mM of aspartic acid, glutamic acid or glycine (Fig. 7). Micrographs of aragonite precipitated at Ω=13 are presented in Castillo Alvarez et al. (2024). In all treatments synthetic aragonite typically forms as radiate clusters of sub-equant pyramidal crystals which nucleate on the existing mineral surface and extend to form points. Aragonite morphology is affected by both Ω and by the addition of amino acids (Fig. 7). At Ω=18 the pyramidal crystals in all treatments

exhibit some porosity and the crystal surfaces are rough. At Ω=7 the crystals are denser and their surfaces are smooth. In the presence of 2 mM aspartic acid aragonites are slightly more tabular (spikier) (Fig. 7 c, d) than without amino acid (Fig. 7 a,b). The addition of glutamic acid and glycine has little effect on aragonite morphology at either Ω (Fig. 7 e-h).

4. Discussion

4.1. Controls on B/Ca in synthetic aragonites precipitated with no amino acids

Our data show that changes in solution $[CO_3^{2-}]$ at constant pH have no significant effect on aragonite B/Ca at pH_{total} 8.20 and 8.41 (Fig. 2b). Only in the experiments with no amino acid at pH 8.59 is a significant (inverse) relationship observed between $[CO_3^{2-}]$ and aragonite B/Ca (Fig. 4b,Table S2). Changes in [DIC], $[HCO_3^-]$ and aragonite precipitation rate also have little effect on aragonite B/Ca (Table 1) as $[CO_3^{2-}]$ and $[HCO_3^-]$ or [DIC] are linearly related at constant pH and because $[CO_3^{2-}]$ and precipitation rate are strongly positively correlated (r^2=0.99) across the entire dataset (Castillo Alvarez et al., 2024).

Aragonite B/Ca is positively correlated with seawater pH (Fig. 2a, Table S2) and with solution B/DIC, $B(OH)_4^-/CO_3^{2-}$, $B(OH)_4^-/HCO_3^-$ and $B(OH)_4^-/(CO_3^{2-})^{0.5}$ (Fig. 3) across precipitations conducted at multiple pH values. However, this relationship is driven by the effect of pH on boron speciation in seawater and the abundance of $B(OH)_4^-$. Normalising aragonite B/Ca to solution $[B(OH)_4^-]$, producing $K_D^{B(OH)4-}$, removes significant differences between pH 8.20 and 8.41 treatments (Fig. 3, Table S3). In other words, changes in aragonite B/Ca in this study are driven by the influence of pH on $B(OH)_4^-$ abundance in seawater and are independent of variations in the DIC species in solution at pH 8.20 and 8.41. Critically, this implies that $B(OH)_4^-$ and CO_3^{2-} (or other DIC species) do not compete for inclusion in the aragonite lattice in most of the precipitations in this study. Only at high pH (pH_{total} = 8.59), do we observe evidence that the 2 anions compete to be incorporated into the lattice.

A comprehensive review of $CaCO_3$ mineral growth and processes affecting B incorporation in $CaCO_3$ is provided by Branson (2018). $CaCO_3$ minerals may grow by one of more of: a) the attachment of single ions to the crystal growth face, b) by the topotactic attachment of entire nano-crystals (de Yoreo et al., 2015) or c) by the attachment of amorphous calcium carbonates (ACC) as reported in coral aragonite biomineralisation (Sun et al., 2020). Prior to attachment, the relevant entity (ion, ACC, nanocrystal) encounters the crystal surface, becomes desolvated (if in ionic form) and bonds with the surface. After attachment, ions may become buried by further growth of the solid, migrate across the surface to other attachment sites or detach back into solution. ACC may also be buried in aragonite before conversion to the mineral phase (Sun et al., 2020).

Boron (and other trace and minor elements) can be viewed as impurities which are incorporated into the aragonite structure in place of the host ions (Ca^{2+} and CO_3^{2-}). Both theoretical calculations (Balan et al., 2016) and studies of B structural state (Sen et al. 1994; Klochko et al., 2009; Noireaux et al. 2015) suggest that $B(OH)_4^-$ is the ion predominantly incorporated into the aragonite by substitution for CO_3^{2-}. The molar ratio of $B(OH)_4^-$: CO_3^{2-} in the solutions of these experiments varies from 1:2 to 1:7 while the ratio of $B(OH)_4^-$: CO_3^{2-} in the solid phase, inferred assuming CO_3^{2-} is equimolar with aragonite Ca^{2+}, ranges from ~1:1500 to 1:3000. This indicates that $B(OH)_4^-$ is much less likely to be incorporated in the lattice than CO_3^{2-}.

In the experiments reported here, solution $[Ca^{2+}]$ is 9–10 mmol kg^{-1} and far exceeds that of $[CO_3^{2-}]$, even in the experiments conducted at the highest $[CO_3^{2-}]$ (up to 1.1 mmol kg^{-1}). Our data are consistent with a model whereby the accumulation of negative anions onto the crystal surface is the rate-limiting step to crystal growth, such that both CO_3^{2-} and $B(OH)_4^-$ are incorporated at the mineral surface in proportion to their abundance in seawater, albeit with different efficiencies i.e. each CO_3^{2-} is more likely to be incorporated than $B(OH)_4^-$. This means that B/Ca of the solid reflects faithfully the $[B(OH)_4^-]$ of the solution independent of $[CO_3^{2-}]$ at pH 8.20 and 8.41.

Aragonite B/Ca is inversely related to both $[CO_3^{2-}]$ and precipitation rate at pH_{total} = 8.59. In experiments at this pH $[CO_3^{2-}]$ is up to 1.1 mmol kg^{-1}, $[B(OH)_4^-]$ is ~ 0.21 mmol kg^{-1} and $[Ca^{2+}]$ is 9.9–10.5 mmol kg^{-1}. Potentially $[B(OH)_4^-]$ exceeds a critical threshold at this point and begins to compete with CO_3^{2-} for attachment to the mineral. Rapid mineral precipitation rates which exceed the rates of ion diffusion in solution, can create boundary layers, both at the mineral surface (Watson 2004) and in the solution adjacent to the mineral (Watson 1996), with different compositions to the bulk mineral and bulk solution. If the impurity ion (in this case $B(OH)_4^-$) is drawn into the mineral at a slower rate than the co-precipitating ion (in this case CO_3^{2-}) then the solution boundary layer becomes enriched in $B(OH)_4^-$ relative to CO_3^{2-} compared to the bulk solution. Aragonite precipitated from this boundary layer will also be enriched in $B(OH)_4^-$ (Watson 1996). More recently, dePaolo (2011) highlighted the importance of the kinetics of ion attachment (and detachment) in mediating relationships between mineral precipitation rate and trace element incorporation. If disequilibria occur on the mineral surface then impurity ions may become buried or entrapped at the mineral surface during rapid precipitation (Watson 2004). These models predict increased impurity ion incorporation at high mineral precipitation rates. This is the opposite to the relationship observed in this study, where aragonite B/Ca decreases at high precipitation rates at pH_{total} 8.59 (Fig. S1). Similarly high precipitation rates in the other pH treatments (8.20 and 8.41) are not associated with significant changes in B incorporation (Fig. S1, Table S2). This suggests that these models, and thereby precipitation rate, do not explain the decrease in aragonite B/Ca observed at high pH and high $[CO_3^{2-}]$.

The attachment of ions to the mineral surface is influenced by the interactions of the ion with other solutes in the solution and with other ions on the mineral surface (dePaolo, 2011). Changes in aragonite precipitation rate or solution $[CO_3^{2-}]$ can drive alterations in the incorporation of other impurity minor/trace elements into aragonite e.g. Ba (Mavromatis et al., 2018) or Mg (Mavromatis et al., 2022). These changes could also influence the attachment of $B(OH)_4^-$. However changes in crystal habit in aragonites precipitated with no amino acid at Ω=7 and Ω=18 (Fig. 7a,b) are not associated with significant variations in aragonite B/Ca (Fig. 2b) or $K_D^{B(OH)4-}$ (Fig. 4b) in this study.

4.2. Comparison with other studies

Our observation that aragonite B/Ca is not affected by seawater $[CO_3^{2-}]$ under some conditions is contrary to previous reports (Holcomb et al., 2016; Allison 2017). Holcomb et al. (2016) reported strong positive correlations between aragonite B/Ca and solution $[B(OH)_4^-]/[CO_3^{2-}]$ and $[B(OH)_4^-]/[CO_3^{2-}]^{0.5}$. However as shown by Fig. 3, these relationships can reflect the increase in seawater $[B(OH)_4^-]$ at high pH. There is a strong positive correlation between seawater pH and $[CO_3^{2-}]$ in the Holcomb et al. (2016) study (Fig. 1) indicating that changes in $[CO_3^{2-}]$ in their study were typically also associated with changes in seawater pH. To compare our data to previous studies we calculate $K_D^{B(OH)4-}$ using the data of both Holcomb et al. (2016) and Mavromatis et al. (2015) and plot these estimates with the data generated in the present study (Fig. 8). We plot K_D from the Holcomb et al. (2016) data as a function of both $[CO_3^{2-}]$ and Ω, as $[Ca^{2+}]$ was not dosed during the Holcomb et al. (2016) precipitations resulting in large variations in solution $[Ca^{2+}]$.

In the Holcomb et al (2016) data, there are no significant relationships between $K_D^{B(OH)4-}$ and $[CO_3^{2-}]$ when $[CO_3^{2-}]$ is < 1000 μmol kg^{-1} (Fig. 8a, r2=0.21, p=0.064, n=17) or between K_D and Ω when Ω < 16 (Fig. 8b, r2=0.11, p=0.16, n=19). These data are in agreement with our study. If the analysis of the Holcomb et al (2016) data is expanded to cover all $[CO_3^{2-}]$ and Ω, then inverse relationships between K_D and both

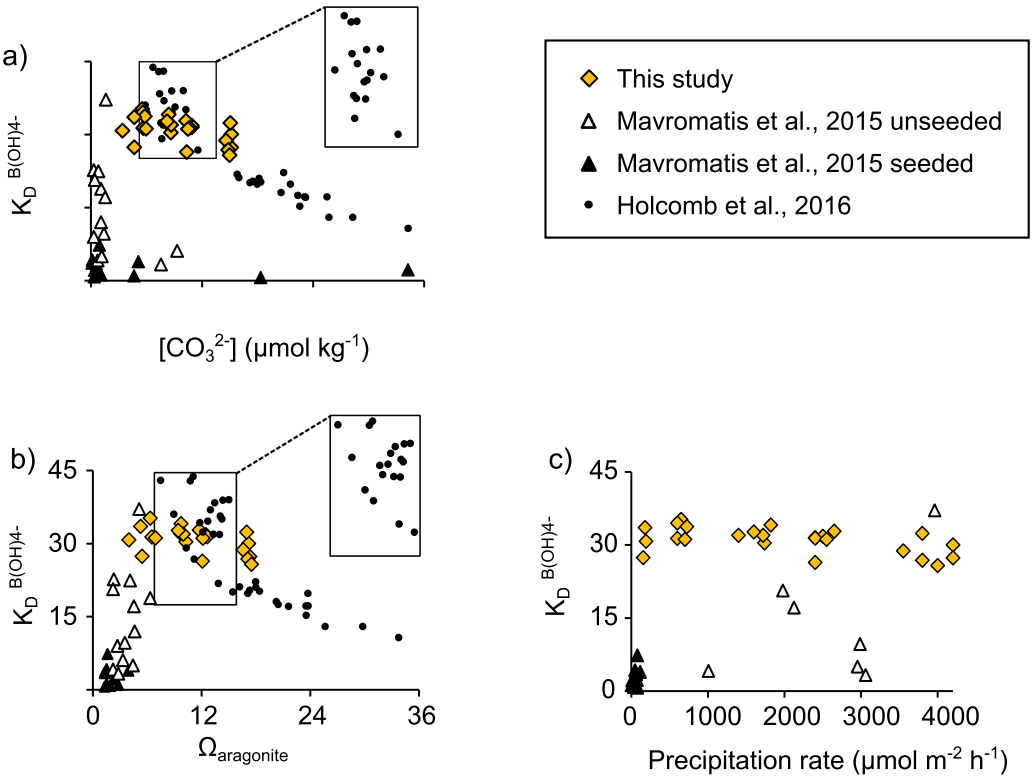

Fig. 8. A comparison of the data generated here with that of Mavromatis et al. (2015) and Holcomb et al. (2016). Data are limited to those conducted at ~ 25 °C, at typical seawater [B] and in the absence of additives. K_D as a function of a) [CO_3^{2-}], b) $\Omega_{aragonite}$ and c) precipitation rate. Insets show the Holcomb et al. dataset at low [CO_3^{2-}] and Ω in the absence of the other studies for clarity. Mavromatis et al. (2015) completed seed and unseeded experiments and both are shown. Precipitation rates for these unseeded experiments were calculated by normalising the Ca^{2+} consumption rate during the titration to the surface area of the final precipitate and assuming that this was representative of the surface area for $CaCO_3$ growth during the titration.

[CO_3^{2-}] and Ω are observed (Fig. 8). In the Holcomb et al. (2016) study, experiments at high [CO_3^{2-}] were usually conducted at high pH (Fig. 1). This supports our conclusion that [CO_3^{2-}] and [$B(OH)_4^-$] may compete for inclusion in the lattice at higher pH. The inverse relationships between K_D and both [CO_3^{2-}] and Ω in the Holcomb et al. (2016) dataset exhibit steeper gradients than suggested by the data in the present study and a one way ANCOVA test indicates that the slopes between K_D and both [CO_3^{2-}] and Ω are significantly different in the Holcomb et al (2016) data compared to the present study ($p = 4.6. \times 10^{-5}$ and 6.4×10^{-5} respectively). This suggests that competition between $B(OH)_4^-$ and [CO_3^{2-}] during precipitation is more intense in the Holcomb et al. (2106) study. In the Holcomb et al (2016) study, precipitations at Ω ≥16 were conducted using seawater with a starting [Ca^{2+}] of ~9.5 mmol kg^{-1}. [Ca^{2+}] was not dosed during the precipitations and [Ca^{2+}] typically dropped by ~35% in the titrations to ~5.9 mmol kg^{-1}. In these high Ω experiments, [CO_3^{2-}] ranged from 1.2 to 2.6 mmol kg^{-1}, so [Ca^{2+}] and [CO_3^{2-}] were more comparable and so it is more likely that competition between B $(OH)_4^-$ and CO_3^{2-} will occur for inclusion in the lattice. In the Holcomb et al (2016) study, almost all precipitations at Ω ≤16 were conducted with higher and more variable starting [Ca^{2+}] (up to 19 mmol kg^{-1}) and further work is required to identify how these changes in [Ca^{2+}] influence boron partitioning.

The aragonite precipitations of Mavromatis et al. (2015) generate highly variable $K_D^{B(OH)4-}$ (Fig. 8). These experiments were conducted in 0.1–0.2 M NaCl solutions, at low $\Omega_{aragonite}$ and span broad ranges of [CO_3^{2-}] (0.01–2.6 mM), [Ca^{2+}] (0.031–4.7mM) and [$B(OH)_4^-$] (0.069–9.9 mM). The highest $K_D^{B(OH)4-}$ calculated from this dataset is 49.9 and is observed in a titration with [CO_3^{2-}] = 0.027mM, [Ca^{2+}] = 2.3 mM and [$B(OH)_4^-$] =0.069 mM. In this titration, as in the present study, the supply of anions to the growing crystal is likely to be the rate-limiting step and competition between $B(OH)_4^-$ and CO_3^{2-} may not occur, generating a K_D that is broadly comparable to those observed in the present study. In contrast, the lowest $K_D^{B(OH)4-}$ (at 0.653) is observed in a titration with [CO_3^{2-}] = 1.4 mM, [Ca^{2+}] = 0.033 mM and [$B(OH)_4^-$] = 9.9 mM. Under these conditions, where the host mineral cation (Ca^{2+}) is lower in concentration than the anion (CO_3^{2-}), competition between $B(OH)_4^-$ and CO_3^{2-} for inclusion in the lattice is likely, reducing the aragonite B/Ca and $K_D^{B(OH)4-}$.

Our observation that precipitation does not typically influence B incorporation in aragonite at pH 8.20 and 8.41 is contrary to a previous report (Mavromatis et al., 2015). This latter study identified a positive relationship between precipitation rate and K_D B/CO_3^{2-} in a series of 7 aragonites (3 seeded and 4 unseeded) precipitated over a relatively narrow pH_{total} range (8.29–8.39). Although this comparison utilised a narrow pH range, solution [$B(OH)_4^-$] varied by x4 between experiments. Further work is required to deconvolve the roles of precipitation rate, pH and solution [$B(OH)_4^-$] in B incorporation in aragonite. Growth rate enhances B incorporation in calcite even at low $\Omega_{calcite}$ (Gabitov et al., 2014; Kaczmarek et al., 2016; Uchikawa et al., 2017). There is evidence that both $B(OH)_4^-$ and $B(OH)_3$ are incorporated in calcite (Uchikawa et al., 2017) suggesting that the incorporation mechanism varies between calcite and aragonite.

4.3. Incorporation of boron in aragonite in the presence of amino acids

$K_D^{B(OH)4-}$ are higher in the presence of 2 mM glutamic acid and glycine compared with no amino acid after correcting for [CO_3^{2-}] or pH (Fig. 6, S1, Table 2) but aspartic acid did not significantly alter B

incorporation (Fig. 6b, Table 2). $K_D^{B(OH)4-}$ are also more variable between replicate precipitations in the presence of aspartic and glutamic acids than without amino acids (Fig. 5 b,c). 2 mM of each of the amino acids reduced aragonite precipitation rates when normalised to Ω in these experiments (Fig. 5a). Amino acids can reduce $CaCO_3$ precipitation rate by either complexing Ca^{2+} in solution (De Stefano et al., 1995), thereby reducing Ω, or by adsorbing to the mineral surface blocking the attachment of host ions (Reddy and Hoch, 2001). Although K_D are significantly increased by the addition of glutamic acid and glycine, the influence of this is relatively small i.e. mean K_D are 14% and 19% higher with glutamic acid and glycine respectively compared to experiments with no amino acid. Similarly, the increase of K_D between pH 8.2 and pH 8.6 is 14% with glycine and 21% with aspartic acid (Fig. 6). Our observation that large reductions in aragonite precipitation rate in response to aspartic acid (Fig. 5a) are not associated with significant changes in K_D (Fig. 6b) supports our conclusion that K_D is not affected by aragonite precipitation rate.

The Mg/Ca of synthetic calcite increases in the presence of glycine and glutamic acid compared with no amino acids, when Ω is corrected to yield similar precipitation rates between experiments (Mavromatis et al., 2017). The authors concluded that the higher Ω required to generate the selected precipitation rate in the presence of amino acids, permitted a rapid precipitation rate at crystal sites which were not blocked by the amino acid and enhanced Mg uptake. This seems an unlikely explanation for the data patterns observed here where increases in precipitation rate are either not related or inversely related to boron incorporation in aragonite (Fig. S1).

It is more likely that $K_D^{B(OH)4-}$ reflects interactions of each specific amino acid with solutes or the aragonite crystal surface. Low concentrations of acidic biomolecules may promote calcite precipitation by reducing the energy required for desolvation of hydrated cations (Elhadj et al., 2006; Stephenson et al., 2008). Aspartic acid is incorporated into aragonite from seawater (Kellock et al., 2020) and density function theory calculations indicate that amino acids preferentially sorb to particular crystal faces in gypsum, altering the attachment of Ca and creating Ca isotopic fractionation (Harouaka et al., 2017). Sulphate and phosphate both inhibit precipitation and increase B/Ca in synthetic calcite possibly because the incorporation of SO_4^{2-} and PO_4^{3-} into the mineral lattice creates deformations which enhance the incorporation of $B(OH)_4^-$ (Uchikawa et al., 2023). Collectively these observations suggest that the amino acids used here can influence both the activities and desolvation of solutes consumed during mineral growth and/or interact with the aragonite growth surface to alter impurity ($B(OH)_4^-$) incorporation. We note that glutamic acid ($C_5H_9NO_4$) and glycine ($C_2H_5NO_2$) are the largest and smallest (respectively) amino acids tested here while aspartic acid ($C_4H_7NO_4$) has a similar structure to glutamic acid but with one fewer methylene bridge. The attachment of amino acids to the existing aragonite growth surface will reflect both the structure of the amino acid, the particular crystal face and the landscape of the mineral surface e.g. the abundance of impurity ions. We find preliminary evidence that K_D is inversely correlated with solution pH in the presence of glycine and aspartic acid. More work is required to identify if this relationship is mediated by solution $[H^+]$ or via changes in the chemistry of the mineral surface. Finally, we observe variations in the morphology of the aragonites precipitated with and without aspartic acid (Fig. 7a-d) as reported by Castillo Alvarez et al. (2024), albeit at different Ω. We note that these variations are not associated with a consistent change in K_D (Fig. 6).

4.4. Relevance for reconstructing coral calcification fluid DIC

The use of coral skeletal B/Ca to reconstruct the DIC chemistry of the coral calcification media assumes that $B(OH)_4^-$ and DIC species compete for inclusion into the lattice (Allison et al., 2014; Holcomb et al., 2016; Allison 2017). Our data (and a re-examination of Holcomb et al., 2016) suggest that these ions only compete at high pH ($pH_{total} = 8.59$) and high

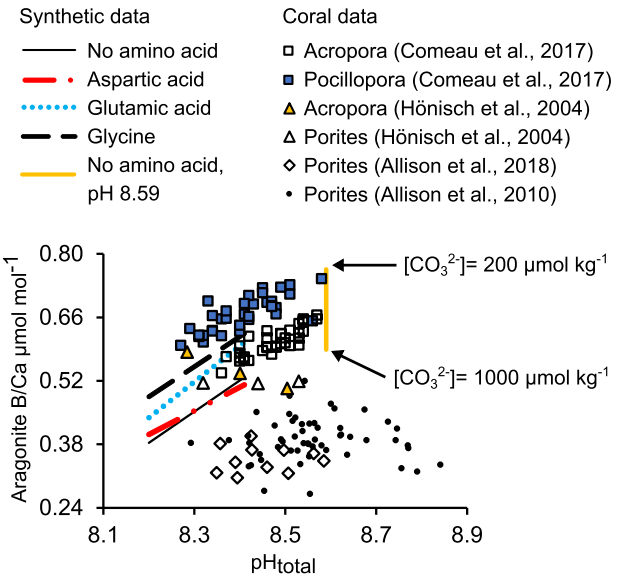

Fig. 9. Predicted relationships between fluid pH and aragonite B/Ca in synthetic precipitates using the K_D estimated in this study (lines). Predicted relationships are shown between pH 8.20 to 8.41 for precipitates with and without amino acids. At pH 8.59 only the relationship without amino acid is shown (for clarity) displaying the influence of $[CO_3^{2-}]$ on K_D at this pH. Observed relationships between coral calcification media pH (estimated from skeletal $\delta^{11}B$) and skeletal B/Ca (using the data of Hönisch et al., 2004, Comeau et al., 2017; Allison et al., 2010, 2018). All coral data are from studies where corals were cultured over a range of seawater pCO_2 with the exception of Allison et al., 2010 which indicates a study of high resolution variations in a coral collected from a reef.

$[CO_3^{2-}]$ (Fig. 8). This pH is at the uppermost limit of conditions reliably measured in the coral calcification media (see introduction) suggesting that aragonite B/Ca does not reflect accurately calcification media DIC in many corals.

To illustrate the implications of our study we use the $K_D^{B(OH)4-}$ calculated in this study to predict aragonite B/Ca at pH_{total} 8.20, 8.41 and 8.59 (Fig. 9). At pH 8.20 and 8.41 we assume that $[CO_3^{2-}]$ has no influence on $K_D^{B(OH)4-}$. For conditions where we observe no significant relationship between K_D and solution pH i.e. in precipitations with either no amino acid or with glutamic acid, we calculate the K_D from the means of the entire dataset i.e. 31.0 for precipitations with no amino acid and 35.5 for precipitations with glutamic acid. For aspartic acid and glycine (where K_D is significantly affected by pH) we use the regression relationships in Fig. 6 to estimate that K_D decreases from 32.5 and 39.2 at pH 8.20 to 30.0 and 36.6 at pH 8.41 for aspartic acid and glycine respectively. At pH 8.59 we calculate $K_D^{B(OH)4-}$ as 35.7 and 27.5 at $[CO_3^{2-}] = 200$ and 1000 respectively (from Fig. 4b) for precipitations with no amino acid. We assume the solution used for precipitation has $[B] = 432.6$ µmol kg^{-1} and that the aragonite formed during precipitation has a mass of 100 g mol^{-1} (equivalent to that of pure $CaCO_3$). We calculate $[B(OH)_4^-]$ using K^*_B (Dickson 1990a) at T=25°C and salinity = 35. We plot aragonite B/Ca as a function of solution pH (Fig. 9). We also plot observed relationships between coral calcification media pH (derived from skeletal $\delta^{11}B$) and skeletal B/Ca from Hönisch et al. (2004), Comeau et al. (2012), Allison et al. (2010) and Allison et al. (2018) onto this graph. The Hönisch et al. (2004) $\delta^{11}B$ data is converted to pH as in Allison (2017).

The synthetic precipitation data predict positive relationships between fluid pH and aragonite B/Ca over the entire pH range (8.20 to 8.59). Similar relationships with similar slopes are reported by Comeau et al. (2017) in an experiment with *Acropora youngei* and *Pocillopora damicornis*. This is encouraging, however fluid pH and aragonite B/Ca

are either inversely related in other studies (e.g. in A*cropora nobilis*, Hönisch et al., 2004) or are not consistently related (Allison et al., 2010, 2018 or in *Porites cyclindrica,* Hönisch et al., 2004). Although CO_3^{2-} may compete with $B(OH)_4^-$ for incorporation into aragonite at pH 8.59, the effect of this on predicted aragonite B/Ca is relatively small because the effect of CO_3^{2-} on $K_D^{B(OH)4-}$ is also small (Fig. 4b). It is unclear why relationships between calcifcation media pH and skeletal B/Ca differ between corals. In coral data, calcification media pH is inferred from skeletal $\delta^{11}B$ analyses and calcification media [B] and $\delta^{11}B$ is assumed to approximate that of seawater. A recent study indicates that $\delta^{11}B$ estimates of coral calcification media are about ~0.4 pH units higher than estimates based on the pH sensitive dye SNARF in the extracellular calcification media (Allison et al., 2023) although the reason for this is unresolved. Coral aragonite may form via an amorphous calcium carbonate precursor (Mass et al., 2017; Sun et al., 2020) as well as by ion-by-ion attachment to the existing skeleton (Sun et al., 2020). The influence of this precursor phase on skeletal B/Ca (and $\delta^{11}B$) is yet to be determined. Resolving the origin of the differences in relationships between calcifcation media pH and skeletal B/Ca in different corals (Fig. 9) is crucial to understanding how boron geochemistry relates to calcification media DIC chemistry.

Our study indicates that simple amino acids can significantly increase B incorporation in aragonite. Coral skeletons are complex composites of aragonite and biomolecules including proteins, polysaccharides and lipids (Falini et al., 2015). Further work is required to explore how these larger biomolecules influence B incorporation in aragonite. We note that the organic content (Tambutté et al., 2015; Coronado et al., 2019) and amino acid concentration (Kellock et al., 2020) of coral skeletons increases in response to elevated seawater pCO_2. $\delta^{11}B$ analyses of the specimens analysed by Kellock et al. (2020) suggests that coral calcifcation media pH is reduced in some of these corals (Allison et al., 2018). If skeletal organic materials enhance the incorporation of boron then this could explain the high skeletal B/Ca observed in corals with low $\delta^{11}B$ calcification media pH (assuming these corals also have high organic contents).

Finally, we note that coral biomineralisation likely occurs in confined areas which may influence the transport of host and impurity ions to the skeletal growth surface. This is at odds with the synthetic experiments where precipitation occurs in a well mixed container. Aragonite precipitation rates may also vary between the synthetic precipitates and coral skeletons but this is difficult to quantify. In massive *Porites* spp. corals, the trabeculae (skeletal rods which make up the majority of the coral skeleton) are typically ≥80 μm wide within 100 μm of the top of the coral skeleton (see Fig. 1 in Allison et al., 2010). Corals of this genus typically extend their skeletons by ≥ 8 mm $year^{-1}$, equivalent to at least 20 μm day^{-1} on average. Assuming that the trabecula increases in diameter as acicular crystals radiate out from a central core point, we infer that the crystals extend by ~8 μm per day, equivalent to an aragonite precipitation rate of ~10,000 μmol/m^{-2}(−|-) $hour^{-1}$, assuming aragonite has a density of 2.94 g cm^{-3}. Aragonite precipitation rates *in vitro* at Ω=12 (the inferred Ω of the coral calcification media, Sevilgen et al., 2019) are ~2000 μmol/m^{-2}(−|-) $hour^{-1}$ (Kellock et al., 2022, Castillo Alvarez et al., 2024) This calculation suggests that aragonite precipitation rates *in vivo* exceed those *in vitro* by some margin. However precipitations *in vitro* are normalised to the total surface area of the seed although it is unlikely that nucleation occurs across all the seed. Rather, nucleation occurs at specific sites e.g. kinks and dislocations (de Yoreo and Vekilov, 2003) and then propagates from these points. For this reason it is not possible to compare directly precipitation rates *in vitro* and *in vivo*.

Whilst the pattern of B/Ca versus reconstructed calcification pH in coral skeletal data remains unexplained, the present study demonstrates that $B(OH)_4^-$ and CO_3^{2-} do not compete for inclusion in the aragonite lattice at pH_{total} 8.20 and 8.41. The pH of tropical coral calcification media ranges from 8.3 to 8.6 in modern day corals (Venn et al., 2011, 2013; Sevilgen et al, 2019) and decreases in response to ocean acidification (Venn et al., 2013, 2019). Within these constraints we conclude that coral skeletal B/Ca may not reflect the concentrations of DIC species at the coral calcification site as suggested previously (e.g. Allison et al., 2014).

5. Conclusions

We explored how pH, [DIC] species and the presence of 3 amino acids affect the incorporation of B in aragonite under conditions likely to occur in tropical coral calcification media. [DIC], $[CO_3^{2-}]$ and $[HCO_3^-]$ have no significant effect on B incorporation at pH_{total} 8.20 and 8.41 and an inverse effect at pH 8.59. This implies that $B(OH)_4^-$ and CO_3^{2-} do not compete with each other for inclusion in the aragonite lattice except at high $[B(OH)_4^-]$ i.e. at high pH. Direct measurements indicates that the pH_{total} of the extracellular calcification media of corals cultured at present day pCO_2 is ~8.3 to ~8.6 (Venn et al., 2011, 2013; Sevilgen et al, 2019) and decreases in corals cultured under ocean acidification conditions (Venn et al., 2013, 2019). This suggests that coral aragonite B/Ca may not reflect the $[CO_3^{2-}]$ chemistry of the coral calcification media. Glutamic acid and glycine enhance the incorporation of B in aragonite but aspartic acid has no measurable effect.

CRediT authorship contribution statement

Cristina Castillo Alvarez: Writing – review & editing, Writing – original draft, Validation, Methodology, Investigation, Formal analysis. **Kirsty Penkman:** Writing – review & editing, Funding acquisition, Conceptualization. **Roland Kröger:** Writing – review & editing, Methodology, Funding acquisition, Conceptualization. **Adrian A. Finch:** Writing – review & editing, Funding acquisition, Conceptualization. **Matthieu Clog:** Writing – review & editing, Funding acquisition, Conceptualization. **Ed Hathorne:** Writing – review & editing, Validation, Methodology, Investigation, Formal analysis. **Nicola Allison:** Writing – review & editing, Writing – original draft, Validation, Supervision, Project administration, Methodology, Investigation, Funding acquisition, Formal analysis, Conceptualization.

Declaration of competing interest

The authors declare that they have no known competing financial interests or personal relationships that could have appeared to influence the work reported in this paper.

Data availability

Data are available through Mendeley Data at https://doi.org/10.17632/cvd66cs5y2.1.

Acknowledgements

This work was supported by the UK Natural Environment Research Council (NE/S001417/1) to NA, KP, RK, MC and AF. We thank Gavin Peters, University of St Andrews, for assistance with BET analyses and Adam Kerrigan, University of York, for support with scanning electron microscopy. We thank 3 anonymous reviewers and the AE for constructive comments that improved the manuscript.

Appendix A. Supplementary material

The supplementary material contains supplementary figures showing the relationships between aragonite B/Ca and precipitation rate in the aragonites produced with no amino acid (Fig. S1) and between $K_D^{B(OH)4-}$ and seawater $[CO_3^{2-}]$ in precipitations with and without amino acids (Fig. S2). The supplementary material contains details of the reference materials analysed with the aragonites (Table S1), the statistical tests of relationships between aragonite B/Ca

and seawater [CO_3^{2-}], pH and precipitation rate (Table S2), the statistical tests of relationships between K_D [B]$_{solid}$ / [$B(OH)_4^-$]$_{solution}$ and seawater [CO_3^{2-}] and pH (Table S3), the statistical tests of relationships between K_D [B]$_{solid}$ / [$B(OH)_4^-$]$_{solution}$ and pH in the presence of amino acids (Table S4) and the statistical tests of relationships between K_D [B]$_{solid}$ / [$B(OH)_4^-$]$_{solution}$ and seawater [CO_3^{2-}] in the presence of amino acids (Table S5). Supplementary material to this article can be found online at https://doi.org/10.1016/j.gca.2024.06.036.

References

Al-Horani, F.A., Al-Moghrabi, S.M., De Beer, D., 2003. The mechanism of calcification and its relation to photosynthesis and respiration in the scleractinian coral *Galaxea fascicularis*. Mar. Biol. 142, 419–426.

Allison, N., 2017. Reconstructing coral calcification fluid dissolved inorganic carbon chemistry from skeletal boron: an exploration of potential controls on coral aragonite B/Ca. Heliyon.

Allison, N., Cohen, I., Finch, A.A., Erez, J., Tudhope, A.W., 2014. Corals concentrate dissolved inorganic carbon to facilitate calcification. Nat. Comm. 5, 1–6.

Allison, N., Cole, C., Hintz, C., Hintz, K., Rae, J., Finch, A., 2018. The effect of ocean acidification on tropical coral calcification: insights from calcification fluid DIC chemistry. Chem. Geol. 497, 162–169.

Allison, N., Finch, A.A., E.I.M.F., 2010. $\delta^{11}B$, Sr, Mg and B in a modern *Porites* coral: the relationship between calcification site pH and skeletal chemistry, Geochim. Cosmochim.Acta, 74, 1790-1800.

Allison, N., Venn, A.A., Tambutté, S., Tambutté, E., Kasemann, S., Wilckens, F., E.i.m.f.,, 2023. A comparison of SNARF-1 and skeletal $\delta^{11}B$ estimates of calcification media pH in tropical coral. Geochim. Cosmochim. Acta 355, 184–194.

Balan, E., Pietrucci, F., Gervais, C., Blanchard, M., Schott, J., Gaillardet, J., 2016. First-principles study of boron speciation in calcite and aragonite. Geochim. Cosmochim. Acta 193, 119–131.

Beck, R., Seiersten, M., Andreassen, J.P., 2013. The constant composition method for crystallization of calcium carbonate at constant supersaturation. J. Cryst. Growth 380, 187–196.

Branson, O., 2018. Boron incorporation into marine $CaCO_3$. In Boron Isotopes: The Fifth Element, pp. 71-105. Cham: Springer International Publishing.

Burton, E.A., Walter, L.M., 1987. Relative precipitation rates of aragonite and Mg calcite from seawater: temperature or carbonate ion control. Geology 15, 111–114.

Cai, W.J., Ma, Y., Hopkinson, B.M., Grottoli, A.G., Warner, M.E., Ding, Q., Hu, X., Yuan, X., Schoepf, V., Xu, H., Han, C., 2016. Microelectrode characterization of coral daytime interior pH and carbonate chemistry. Nat. Comm. 7, 11144.

Castillo Alvarez, C.C., Penkman, K., Kröger, R., Finch, A.A., Clog, M., Brasier, A., Still, J., Allison, N., 2024. Insights into the response of coral biomineralisation to environmental change from aragonite precipitations *in vitro*. Geochim. Cosmochim. Acta.

Comeau, S., Cornwall, C.E., McCulloch, M.T., 2017. Decoupling between the response of coral calcifying fluid pH and calcification to ocean acidification. Sci. Rep. 7, 7573.

Coronado, I., Fine, M., Bosellini, F.R., Stolarski, J., 2019. Impact of ocean acidification on crystallographic vital effect of the coral skeleton. Nat. Comm. 10, 1–9.

Cuif, J.P., Dauphin, Y., Berthet, P., Jegoudez, J., 2004. Water and organic compounds in coral skeletons: quantitative thermogravimetry coupled to infrared absorption spectrometry. Geochem., Geophys., Geosyst. 5, 11.

De Stefano, C., Foti, C., Gianguzza, A., Rigano, C., Sammartano, S., 1995. Chemical speciation of amino acids in electrolyte solutions containing major components of natural fluids. Chem. Speciation & Bioavailability 7, 1–8.

de Yoreo, J.J., Gilbert, P.U.P.A., Sommerdijk, N.A.J.M., Penn, R.L., Whitelam, S., Joester, D., Zhang, H., Rimer, J.D., Navrotsky, A., Banfield, J.F., Wallace, A.F., Michel, F.M., Meldrum, F.C., Cölfen, H., Dove, P.M., 2015. Crystallization by particle attachment in synthetic, biogenic, and geologic environments. Science 349, aaa6760.

De Yoreo, J.J., Vekilov, P.G., 2003. Principles of crystal nucleation and growth. Rev. Mineral. Geochem. 54, 57–93.

DePaolo, D.J., 2011. Surface kinetic model for isotopic and trace element fractionation during precipitation of calcite from aqueous solutions. Geochim. Cosmochim. Acta 75, 1039–1056.

Dickson, A.G., 1990a. Thermodynamics of the dissociation of boric acid in synthetic seawater from 273.15 to 318.15 K. Deep Sea Res. Part A Oceanogr. Res. Pap. 37, 755–766.

Dickson, A.G., 1990b. Standard potential of the reaction - AgCl(S)+1/2H-2(g)=AG(s)+HCL(aq) and the standard acidity constant of the ion HSO4- in synthetic sea-water from 273.15-K to 318.15-K. J. Chem. Thermodyn. 22, 113–127.

Elhadj, S., De Yoreo, J.J., Hoyer, J.R., Dove, P.M., 2006. Role of molecular charge and hydrophilicity in regulating the kinetics of crystal growth. Proc. Natl. Acad. Sci. 103, 19237–19242.

Enmar, R., Stein, M., Bar-Matthews, M., Sass, E., Katz, A., Lazar, B., 2000. Diagenesis in live corals from the Gulf of Aqaba. I. The effect on paleo-oceanography tracers. Geochim. Cosmochim. Acta 64, 3123–3132.

Falini, G., Fermani, S., Goffredo, S., 2015. Coral biomineralization: A focus on intra-skeletal organic matrix and calcification. Semin. Cell Dev. Biol. 46, 17–26.

Gabitov, R.I., Rollion-Bard, C., Tripati, A., Sadekov, A., 2014. In situ study of boron partitioning between calcite and fluid at different crystal growth rates. Geochim. Cosmochim. Acta 137, 81–92.

Harouaka, K., Kubicki, J.D., Fantle, M.S., 2017. Effect of amino acids on the precipitation kinetics and Ca isotopic composition of gypsum. Geochim. Cosmochim. Acta 218, 343–364.

Hathorne, E.C., Gagnon, A., Felis, T., Adkins, J., Asami, R., Boer, W., Caillon, N., Case, D., Cobb, K.M., Douville, E., Demenocal, P., 2013. Interlaboratory study for coral Sr/Ca and other element/Ca ratio measurements. Geochem. Geophys. Geosyst. 14, 3730–3750.

Holcomb, M., Venn, A.A., Tambutté, E., Tambutté, S., Allemand, D., Trotter, J., McCulloch, M., 2014. Coral calcifying fluid pH dictates response to ocean acidification. Sci. Rep. 4, 5207.

Holcomb, M., DeCarlo, T.M., Gaetani, G.A., McCulloch, M., 2016. Factors affecting B/Ca ratios in synthetic aragonite. Chem. Geol. 437, 67–76.

Hönisch, B., Hemming, N.G., Grottoli, A.G., Amat, A., Hanson, G.N., Bijma, J., 2004. Assessing scleractinian corals as recorders for paleo-pH: empirical calibration and vital effects. Geochim. Cosmochim. Acta 68, 3675–3685.

Kaczmarek, K., Nehrke, G., Misra, S., Bijma, J., Elderfield, H., 2016. Investigating the effects of growth rate and temperature on the B/Ca ratio and $\delta^{11}B$ during inorganic calcite formation. Chem. Geol. 421, 81–92.

Kellock, C., Cole, C., Penkman, K., Evans, D., Kröger, R., Hintz, C., Hintz, K., Finch, A., Allison, N., 2020. The role of aspartic acid in reducing coral calcification under ocean acidification conditions. Sci. Rep. 10, 12797.

Kellock, C., Castillo Alvarez, M.C., Finch, A., Penkman, K., Kröger, R., Clog, M., Allison, N., 2022. Optimising a method for aragonite precipitation in simulated biogenic calcification media. PLoS One 17, e0278627.

Klochko, K., Cody, G.D., Tossell, J.A., Dera, P., Kaufman, A.J., 2009. Re-evaluating boron speciation in biogenic calcite and aragonite using ^{11}B MAS NMR. Geochim. Cosmochim. Acta 73, 1890–1900.

Lee, K., Kim, T.W., Byrne, R.H., Millero, F.J., Feely, R.A., Liu, Y.M., 2010. The universal ratio of boron to chlorinity for the North Pacific and North Atlantic oceans. Geochim. Cosmochim. Acta 74, 1801–1811.

Lueker, T.J., Dickson, A.G., Keeling, C.D., 2000. Ocean pCO_2 calculated from dissolved inorganic carbon, alkalinity, and equations for K_1 and K_2: validation based on laboratory measurements of CO_2 in gas and seawater at equilibrium. Mar. Chem. 70, 105–119.

Mass, T., Drake, J.L., Haramaty, L., Kim, J.D., Zelzion, E., Bhattacharya, D., Falkowski, P. G., 2013. Cloning and characterization of four novel coral acid-rich proteins that precipitate carbonates *in vitro*. Curr. Biol. 23, 1126–1131.

Mass, T., Giuffre, A.J., Sun, C.-Y., Stifler, C.A., Frazier, M.J., Neder, M., Tamura, N., Stan, C.V., Marcus, M.A., Gilbert, P.U.P.A., 2017. Amorphous calcium carbonate particles form coral skeletons. Proc. Nat. Acad. Sci. 114, E7670–E7678.

Mavromatis, V., Montouillout, V., Noireaux, J., Gaillardet, J., Schott, J., 2015. Characterization of boron incorporation and speciation in calcite and aragonite from co-precipitation experiments under controlled pH, temperature and precipitation rate. Geochim. Cosmochim. Acta 150, 299–313.

Mavromatis, V., Immenhauser, A., Buhl, D., Purgstaller, B., Baldermann, A., Dietzel, M., 2017. Effect of organic ligands on Mg partitioning and Mg isotope fractionation during low-temperature precipitation of calcite in the absence of growth rate effects. Geochim. Cosmochim. Acta 207, 139–153.

Mavromatis, V., Goetschl, K.E., Grengg, C., Konrad, F., Purgstaller, B., Dietzel, M., 2018. Barium partitioning in calcite and aragonite as a function of growth rate. Geochim. Cosmochim. Acta 237, 65–78.

Mavromatis, V., Brazier, J.M., Goetschl, K.E., 2022. Controls of temperature and mineral growth rate on Mg incorporation in aragonite. Geochim. Cosmochim. Acta 317, 53–64.

McCulloch, M.T., D'Olivo, J.P., Falter, J., Holcomb, M., Trotter, J.A., 2017. Coral calcification in a changing world and the interactive dynamics of pH and DIC upregulation. Nat. Comm. 8, 15686.

Millero, F.J., 2013. Chemical Oceanography, 4th ed. CRC Press, Boca, Raton, FL.

Mitsuguchi, T., Uchida, T., Matsumoto, E., 2010. Na/Ca variability in coral skeletons. Geochem. J. 44, 261–273.

Morse, J.W., Arvidson, R.S., Lüttge, A., 2007. Calcium carbonate formation and dissolution. Chem. Rev. 107, 342–381.

Mucci, A., 1983. The solubility of calcite and aragonite in seawater at various salinities, temperatures, and one atmosphere total pressure. Am. J. Sci. 283, 780–799.

Noireaux, J., Mavromatis, V., Gaillardet, J., Schott, J., Montouillout, V., Louvat, P., Rollion-Bard, C., Neuville, D., 2015. Crystallographic control on the boron isotope paleo-pH proxy. Earth Planet. Sci. Lett. 430, 398–407.

Pierrot, D., Lewis, E.D., Wallace, W.R., 2006. MS Excel Program Developed for CO_2 System Calculations. Oak Ridge National Laboratory.

Ram, S., Erez, J., 2023. Anion elements incorporation into corals skeletons: experimental approach for biomineralization and paleo-proxies. PNAS 120 e2306627120.

Reddy, M.M., Hoch, A.R., 2001. Calcite crystal growth rate inhibition by polycarboxylic acids. J. Colloid Interface Sci. 235, 365–370.

Rollion-Bard, C., Chaussidon, M., France-Lanord, C., 2003. pH control on oxygen isotopic composition of symbiotic corals. Earth Planet. Sci. Lett. 215, 275–288.

Rosenthal, Y., Field, M.P., Sherrell, R.M., 1999. Precise determination of element/calcium ratios in calcareous samples using sector field inductively coupled plasma mass spectrometry. Anal. Chem. 71, 3248–3253.

Sen, S., Stebbins, J., Hemming, N., Ghosh, B., 1994. Coordination environments of B impurities in calcite and aragonite polymorphs: a ^{11}B MAS NMR study. Am. Mineral. 79, 819–825.

Sevilgen, D.S., Venn, A.A., Hu, M.Y., Tambutté, E., de Beer, D., Planas-Bielsa, V., Tambutté, S., 2019. Full in vivo characterization of carbonate chemistry at the site of calcification in corals. Sci. Adv. 5, p.eaau7447.

Sinclair, D.J., 2005. Correlated trace element "vital effects" in tropical corals: a new geochemical tool for probing biomineralization. Geochim. Cosmochim. Acta 69, 3265–3284.

Spurgeon, J.P., 1992. The economic valuation of coral reefs. Mar. Pollut. Bull. 24, 529–536.

Stephenson, A.E., DeYoreo, J.J., Wu, L., Wu, K.J., Hoyer, J., Dove, P.M., 2008. Peptides enhance magnesium signature in calcite: insights into origins of vital effects. Science 322, 724–727.

Stewart, J.A., Christopher, S.J., Kucklick, J.R., Bordier, L., Chalk, T.B., Dapoigny, A., Douville, E., Foster, G.L., Gray, W.R., Greenop, R., Gutjahr, M., 2021. NIST RM 8301 boron isotopes in marine carbonate (simulated coral and foraminifera solutions): inter-laboratory $\delta^{11}B$ and trace element ratio value assignment. Geostand. Geoanal. Res. 45, 77–96.

Sun, C.Y., Stifler, C.A., Chopdekar, R.v., Schmidt, C.A., Parida, G., Schoeppler, V., Fordyce, B.I., Brau, J.H., Mass, T., Tambutté, S., Gilbert P.U.P.A., 2020. From particle attachment to space-filling coral skeletons, Proc. Natl. Acad. Sci. USA, 117, 30159–30170.

Tambutté, E., Venn, A.A., Holcomb, M., Segonds, N., Techer, N., Zoccola, D., Allemand, D., Tambutté, S., 2015. Morphological plasticity of the coral skeleton under CO_2 driven seawater acidification. Nat. Comm. 6, 1–9.

Uchikawa, J., Penman, D.E., Zachos, J.C., Zeebe, R.E., 2015. Experimental evidence for kinetic effects on B/Ca in synthetic calcite: implications for potential $B(OH)_4^-$ and $B(OH)_3$ incorporation. Geochim. Cosmochim. Acta 150, 171–191.

Uchikawa, J., Harper, D.T., Penman, D.E., Zachos, J.C., Zeebe, R.E., 2017. Influence of solution chemistry on the boron content in inorganic calcite grown in artificial seawater. Geochim. Cosmochim. Acta 218, 291–307.

Uchikawa, J., Penman, D.E., Harper, D.T., Farmer, J.R., Zachos, J.C., Planavsky, N.J., Zeebe, R.E., 2023. Sulfate and phosphate oxyanions alter B/Ca and $\delta^{11}B$ in inorganic calcite at constant pH: crystallographic controls outweigh normal kinetic effects. Geochim. Cosmochim. Acta 343, 353–370.

Venn, A.A., Tambutté, E., Holcomb, M., Allemand, D., Tambutté, S., 2011. Live tissue imaging shows reef corals elevate pH under their calcifying tissue relative to seawater. PLoS One 6, e20013.

Venn, A.A., Tambutté, E., Holcomb, M., Laurent, J., Allemand, D., Tambutté, S., 2013. Impact of seawater acidification on pH at the tissue-skeleton interface and calcification in reef corals. PNAS 110, 1634–1639.

Venn, A.A., Tambutté, E., Caminiti-Segonds, N., Techer, N., Allemand, D., Tambutté, S., 2019. Effects of light and darkness on pH regulation in three coral species exposed to seawater acidification. Sci. Rep. 9, 1–12.

Watson, E.B., 1996. Surface enrichment and trace-element uptake during crystal growth. Geochim. Cosmochim. Acta 60, 5013–5020.

Watson, E., 2004. A conceptual model for near-surface kinetic controls on the trace-element and stable isotope composition of abiogenic calcite crystals. Geochim. Cosmochim. Acta 68, 1473–1488.